Paper

Int'l J. of Aeronautical & Space Sci. 17(1), 80–88 (2016)
DOI: http://dx.doi.org/10.5139/IJASS.2016.17.1.80

IJASS
International Journal of Aeronautical and Space Sciences

Feasibility Study on Tropospheric Attenuation Effect of Ku/V Band Signal for Korean Satellite Navigation System

Jungkeun Park*, Young Jae Lee and Moonseok Choi*****

Konkuk University, Seoul 05029, Republic of Korea

Jae-Gyu Jang****

Agency for Defense Development, Daejeon 34186, Republic of Korea

Sangkyung Sung*****

Konkuk University, Seoul 05029, Republic of Korea

Abstract

For next generation global navigation satellite systems, new carrier frequencies in Ku/V band are expected to emerge as a promising alternative to the current frequency windows in L band as they get severely congestive. In the case of higher frequency bands, signal attenuation phenomenon through the atmosphere is significantly different from the L band signal propagation. In this paper, a fundamental investigation is carried out to explore the Ku/V band as a candidate frequency band for a new global satellite navigation carrier signal, wherein specific attention is given to the effects of the dominant attenuation factors through the tropospheric propagation path. For a specific application, a candidate orbit preliminarily designed for the Korean regional satellite navigation system is adapted. Simulation results summarize that the Ku band can provide a promising satellite navigation implementation considering the present satellite's power budget, while the V band still requires technical advances in satellite transceiver system implementations.

Key words: global navigation satellite system, millimeter wave, attenuation, tropospheric propagation, Korean satellite navigation system

1. Introduction

In designing a global navigation satellite system (GNSS), the allocation of the fundamental carrier frequency within the limited frequency band is the most essential factor for the low level signal transmission. It is widely known that the current frequency band for GNSS is very crowded because of the limited frequency ranges available for assignment within the L band from 1164 MHz to 1610 MHz; specifically, the L1 band (1559~1610 MHz), L2 band (1215~1240 MHz), and L5 band (1164~1215 MHz). These frequency bands for GNSS belong to the radio-navigation satellite service (RNSS) band as designated by the international telecommunication union radio communication sector (ITU-R). L1 is an old frequency band for RNSS, while L2 and L5 are relatively new RNSS bands, which have also been allocated for the aeronautical radio navigation service (ARNS) system. Practically, various GNSS systems under operation or planned for future deployment in these limited frequency bands utilize different signal-in-space designs and use varied communication techniques for signal modulation and spreading code. However, as the number of GNSS systems increase, each GNSS signal experiences mutual radio wave interference, which severely degrades the receiver performance in signal acquisition and tracking. Also,

* Associate Professor
** Ph. D Student
*** Professor
**** Ph. D
***** Professor, Corresponding author: sksung@konkuk.ac.kr

Received: August 3, 2015 Revised: October 1, 2015 Accepted: October 14, 2015

http://ijass.org pISSN: 2093-274x eISSN: 2093-2480

inter-system interference between GNSS systems and other ARNS systems present significant challenges in guaranteeing system performance.

In this respect, future GNSS systems under development attempt to employ a relatively less congestive frequency band for the signal-in-space design [1]. Currently, the international regulation on radio waves for satellite communication and broadcasting service has allocated the S band (2483.5~2500 MHz) and C band (uplink: 5000~5010 MHz, downlink: 5010~5030 MHz) for RNSS service. Several research results have been presented that examine the prospects of band feasibility and technically analyze the pros and cons in terms of propagation and tracking performance [2-4]. These frequency bands having several tens of MHz bandwidth may serve as alternative choices for the future GNSS signal design. However, there still exists the significant challenge of a very strict near-band interference requirement. For instance, radio astronomy demands an extremely low power flux density requirement for downlink channel of the C band, while microwave landing system near uplink channel of the C band demands significant aggregate power flux density requirement. Moreover, the upcoming GNSS systems including modernized GPS, Galileo, and COMPASS systems have disclosed experimental results using prototype transceiver system in these bands. Thus, the space for choosing C and S bands in future GNSS systems is also marginal.

Consequently, in view of a national GNSS or an augmented system design around Korean and north-eastern Asian region that will be in operation around 2025~2030, a preliminary study on a new frequency band is essential [1]. Thus, this paper aims to discover, for the first time, the feasibility of a higher frequency band for a next generation Korean GNSS system, by suggesting specific frequency range around millimeter wavelength and illustrating its signal propagation phenomena through system engineering analysis. The tropospheric attenuation factors are primarily investigated because of their dominant effect during signal propagation.

The rest of the paper is organized as follows: Section 2 briefly describes the band plan for GNSS system regulated by the ITU-R and aims to discover a candidate frequency band in the higher frequency domain for the future Korean satellite navigation system (KNS). In Section 3, certain essential signal attenuation factors of near-millimeter wave passing through a tropospheric propagation path are illustrated. It includes a detailed presentation of the gas absorption and rain attenuation models considering a GNSS signal design environment. Section 4 provides simulation results of the space-earth link simulator by using the presented attenuation models and generating virtual orbital trajectory for navigation satellite, which further facilitates space-to-earth link budget analysis. Finally, Section 5 concludes the paper with a discussion of our current research.

2. GNSS band plan and observation

Frequency band allocation for GNSS service is fundamentally governed by the regulations and technical documents published by ITU-R. The latest ITU-R RR (Radio Regulation) published in 2012 contains band allocations for RNSS ranging from 1.2 GHz to 265 GHz in maximum. Among these, low frequency bands including L, S, and C bands are extensively employed by the service providers for operating system design and implementation. As compared to the low frequency bands, higher frequency bands such as Ku and V bands have attracted less interest due to their immature technical readiness of the transmitter, receiver, and antenna hardware technologies. Nevertheless, as the low frequency band is excessively occupied by various GNSS systems, even with a narrow bandwidth the necessity for low interference and wider bandwidth is greatly increased. Fig. 1 shows the frequency allocation table for conventional RNSS systems in the L, C, and S bands. For frequency allocation, the world has been divided into three regions, where Korea lies in Region 3. All the conventional frequency bands are allocated to radio navigation, radio location, and radio determination satellite services, and are mostly used by present global GNSS operators. As the ARNS services overlap in these bands as a co-primary or secondary service plan, each band has a very limited bandwidth with strong constraints being imposed on the near-band interference.

In contrast, Fig. 2 depicts the allocated RNSS frequency

	Region 1	Region 2	Region 3
1164 ~ 1215 MHz L5 band	AERONAUTICAL RADIONAVIGATION RADIONAVIGATION-SATELLITE (space-to-Earth) (space-to-space)		
1215 ~ 1300 MHz L2/E6 band	EARTH EXPLORATION-SATELLITE (active) RADIOLOCATION RADIONAVIGATION-SATELLITE (space-to-Earth) (space-to-space) SPACE RESEARCH (active)		
1559 ~ 1610 MHz L1 band	AERONAUTICAL RADIONAVIGATION RADIONAVIGATION-SATELLITE (space-to-Earth) (space-to-space)		
2483.5 ~ 2500 MHz S band	FIXED MOBILE MOBILE-SATELLITE (space-to-Earth) RADIODETERMINATIONSAT ELLITE (space-to-Earth) Radiolocation	FIXED MOBILE MOBILE-SATELLITE (space-to-Earth) RADIOLOCATION RADIODETERMINATIONSAT ELLITE (space-to-Earth)	FIXED MOBILE MOBILE-SATELLITE (space-to-Earth) RADIOLOCATION RADIODETERMINATIONSAT ELLITE (space-to-Earth)
5010 ~ 5030 MHz C band	AERONAUTICAL MOBILE-SATELLITE (R) AERONAUTICAL RADIONAVIGATION RADIONAVIGATION-SATELLITE (space-to-Earth) (space-to-space)		

Fig. 1. Frequency allocation table for conventional RNSS systems (Courtesy of the ITU-R Radio Regulation, 2012).

band above 10 GHz, which implies a short wavelength between centimeter and millimeter. RNSS band allocation above the V band is not considered in this paper and is left for future study. The higher frequency band consists of two candidates; one in Ku band and the other in V band. In Fig. 2, it is observed that the RNSS service is allocated in the Ku and V bands, even though it is co-located with fixed satellite service throughout the global regions. The available bandwidth of about 100 MHz in the Ku band is much wider as compared to the conventional band allocated in the low frequency band as shown in Fig. 1. A constraint on the radio service in the Ku band is that the frequency band 14.3-14.4 GHz shall be used by the radio navigation service to provide sufficient protection to space stations of the fixed-satellite service. Furthermore, the second candidate for RNSS that is allocated in the V band provides better flexibility with much larger bandwidth, despite its technical complexity in hardware implementation. Similarly, a constraint on the radio navigation service in the V band is that stations in the land mobile service should be operated such that they do not cause any harmful interference to the space radio communication services within the allocated band [5]. Since the bandwidth allocated for RNSS in Ku and V band is 100 MHz and several hundred MHz, respectively, the increased design freedom in navigation message and space signal structure will bring a notable performance enhancement as compared with the current deployments. For instance, a longer and optimized spreading code can be adapted with an arbitrary code length; a multipath robust modulation method based on much wider bandwidths such as a multi-carrier modulation scheme can be employed; better spectral distribution can be achieved to avoid excessive aggregated power flux density on a ground receiver, etc. In this background, this paper investigates the tropospheric attenuation effect on the higher frequency band signal as a future candidate for Korean GNSS system design.

	Region 1	Region 2	Region 3
14.3 ~ 14.4 GHz Ku band	FIXED FIXED-SATELLITE (Earth-to-space) MOBILE except ARM Mobile-satellite (Earth-to-space) Radionavigation-satellite	FIXED-SATELLITE (Earth-to-space) MOBILE except ARM Mobile-satellite (Earth-to-space) Radionavigation-satellite	FIXED FIXED-SATELLITE (Earth-to-space) MOBILE except ARM Mobile-satellite (Earth-to-space) Radionavigation-satellite
43.5 ~ 47 GHz Lower V band	MOBILE MOBILE-SATELLITE RADIONAVIGATION RADIONAVIGATION-SATELLITE		
66 ~ 71 GHz Upper V band	MOBILE MOBILE-SATELLITE RADIONAVIGATION RADIONAVIGATION-SATELLITE		

Fig. 2. Frequency allocation table in Ku and V band for RNSS (Courtesy of the ITU-R Radio Regulation, 2012).

3. Attenuation model for Ku/V band

This section describes the major signal fading factors of millimeter wave passing through tropospheric space. Mathematical models for each of the signal fading factors are derived and their effects on millimeter wave propagation are described [6-11, 21, 22]. For comprehensive analysis, the most conservative computation method is employed in combining the loss and propagation effects [12].

3.1 Free space loss

Free space loss is the principal signal attenuation factor for satellite GNSS signal. It is the loss of signal strength when a signal propagates through free space. The free space loss is given by

$$FSL = \left(\frac{4\pi R}{\lambda}\right)^2 = \left(\frac{4\pi Rf}{c}\right)^2 \tag{1}$$

where λ is the signal wavelength, f is the frequency of the signal, R is the distance between the two antennas, and c is the speed of light. It is proportional to the square of line-of-sight distance between the transmitter and receiver antennas and also proportional to the square of the frequency of the signal. Taking logarithm on both sides, the following attenuation factor in dB is obtained where f is in GHz and R in km.

$$A_F = 92.4 + 20\log f + 20\log R \tag{2}$$

3.2 Gaseous absorption

The gaseous absorption arises by molecular resonance when a signal propagates in the troposphere. In this atmospheric region, oxygen and water vapors result in significant molecular resonance that causes the attenuation of a signal. The specific attenuation (dB/km) is obtained by line-by-line calculation that is the summation of individual resonance lines at a specific pressure, temperature, and humidity. It is given by

$$\gamma = \gamma_o + \gamma_w = 0.1820 f N''(f) \qquad \text{(dB/km)} \tag{3}$$

where γ_o and γ_w are the specific attenuation due to dry air and water vapor, respectively and f is the frequency in GHz. $N''(f)$ is the imaginary part of the frequency-dependent complex refractivity and is given by the following line-by-line summation.

$$N''(f) = \sum_i S_i F_i + N''_D(f) \tag{4}$$

DOI: http://dx.doi.org/10.5139/IJASS.2016.17.1.80

where S_i is the strength of the i-th line and F_i is the line shape factor. $N_D''(f)$ is the dry continuum due to pressure-induced nitrogen absorption and Debye spectrum [13, 15].

The slant path attenuation is obtained by dividing the atmosphere into layers and integrating the specific attenuation along the path through the layers considering different pressure, temperature, and humidity in each layer. Specifically, the atmosphere is divided into n layers assuming that the atmospheric conditions are constant at each layer. Then, the slant path attenuation is derived by

$$A_G = \sum_{n=1}^{k} a_n \gamma_n \qquad \text{(dB)} \tag{5}$$

where a_n is the path length through the n-th layer and γ_n is the specific attenuation in the n-th layer that is calculated by Eq. (3). The path length a_n depends on the thickness of the n-th layer and the incidence angle of the signal into the n-th layer. The thickness of the layers is chosen to increase exponentially as the altitude increases because there are greater changes in the atmospheric conditions near the ground level than at higher altitudes. The incidence angle in each layer changes according to Snell's law because each layer has a different refractive index [20].

3.3 Attenuation by clouds and fog

For clouds or fog, the Rayleigh approximation can be applied at frequencies below 200 GHz [16]. The specific attenuation γ_c within a cloud or fog can be expressed as

$$\gamma_c = K_l M \qquad \text{(dB/km)} \tag{6}$$

where K_l is the specific attenuation coefficient and M is the liquid water density in the cloud or fog. Based on the Rayleigh model, the specific attenuation coefficient is calculated by

$$K_l = \frac{0.819 f}{\varepsilon''(1+\eta^2)} \qquad \text{(dB/km)/(g/cm}^3\text{)} \tag{7}$$

where f is the frequency in GHz and η is the ratio of the real (ε') and imaginary (ε'') part of the complex dielectric permittivity of water that is given by $(2+\varepsilon')/\varepsilon''$. The complex dielectric permittivity constant depends on the temperature T and the vacuum permittivity ε_0.

The total slant path attenuation due to clouds and fog is obtained using statistical data of liquid water distribution. The slant path attenuation is given by

$$A_C = \frac{L_{red} K_l}{\sin\theta} \qquad \text{(dB)} \tag{8}$$

where θ is the elevation angle ranging from 5 to 90 degree and Kl is calculated from Eq. (7) for a water temperature of 0 °C. L_{red} (kg/m^2) is the total columnar content of liquid water reduced to a temperature of 0°C. For a specific longitude and latitude, its yearly or monthly average values are provided in [16] with the exceedance probabilities.

3.4 Rain attenuation

The slant path attenuation due to rain can be calculated using the rainfall rate, elevation angle, specific attenuation, and horizontal and vertical adjustment factors. If reliable long-term statistical attenuation data are unavailable, the slant path attenuation for the rainfall rate ranging from 0.001% to 5% can be estimated from the rainfall rate exceeded for 0.01% of an average year. First, the specific attenuation γ_R can be obtained by

$$\gamma_R = k(R_{0.01})^{\alpha} \qquad \text{(dB/km)} \tag{9}$$

where k and α are frequency-dependent coefficients that can be obtained from [14] and $R_{0.01}$ is the rainfall rate exceeded for 0.01% of an average year. This rainfall rate can be obtained from local data sources or long-term statistics provided by [18].

Further, the effective path length L_E is calculated by

$$L_E = L_R \nu_{0.01} \qquad \text{(km)} \tag{10}$$

where $\upsilon_{0.01}$ is the vertical adjustment factor for 0.01% of the time and L_R is calculated from the slant path length L_S and the rain height h_R [19].

Finally, the slant path attenuation exceeded for 0.01% of an average year can be obtained by multiplying the specific attenuation and the effective path length as below.

$$A_{0.01} = \gamma_R L_E \qquad \text{(dB)} \tag{11}$$

The above equation provides only the predicted attenuation exceeded for 0.01% of an average year. For an arbitrary probability p in the range 0.001% to 5%, the estimated slant path attenuation due to rain is obtained by using $A_{0.01}$.

$$A_R = A_{0.01}\left(\frac{p}{0.01}\right)^{-(0.655+0.033\ln(p)-0.045\ln(A_{0.01})-\beta(1-p)\sin\theta)} \qquad \text{(dB)} \tag{12}$$

where

$$\beta = \begin{cases} 0 & \text{if } p \geq 1\% \text{ or } |\varphi| \geq 36° \\ -0.005(|\varphi|-36) & \text{if } p < 1\% \text{ and } |\varphi| < 36° \text{ and } \theta \geq 25° \\ -0.005(|\varphi|-36)+1.8-4.25\sin\theta & \text{otherwise} \end{cases}$$

3.5 Scintillation effect

Scintillation refers to the rapid signal fluctuations in amplitude and phase of propagating signals. It can be categorized as ionospheric and tropospheric scintillation depending on the media that causes the fluctuation. One is due to the electron density fluctuation and the other is due to the refractive index fluctuation. In millimeter wave propagation, the tropospheric scintillation is dominant due to the refractive index variation in the first few kilometers of altitude while the ionospheric scintillation is negligible over the frequencies of 6 GHz.

To calculate the attenuation caused by tropospheric scintillation, prediction models for statistical distribution of scintillation are used. The attenuation due to scintillation is given by

$$A_S = a(p)\sigma_{ref} f^{7/12} \frac{g(x)}{(\sin\theta)^{1.2}} \quad \text{(dB)} \tag{13}$$

where $a(p)$ is the time percentage factor, σ_{ref} is the standard deviation of the reference signal amplitude that is related to the wet term of radio wave refractive index N_{wet}, f is the frequency in GHz, $g(x)$ is the antenna averaging factor, x is given by $1.22D_{eff}^2(f/L)$, D_{eff} is the effective antenna diameter, L is the effective path length, and θ is the elevation angle.

3.6 Ionospheric effect

Ionospheric absorption is due to the interaction between electromagnetic waves and the free electrons in the ionosphere, which can interfere with radio transmission [17]. Table 1 explains the fundamental molecular physical phenomena in ionospheric propagation for various frequency ranges. In equatorial and mid-latitude region, the ionospheric absorption is negligible for frequencies above 70 MHz, while in high latitude region, it increases due to polar cap and auroral events. Auroral absorption results from an increase in the electron concentration and polar cap absorption occurs due to high solar activity. However, for near millimeter wave ranges, ionospheric absorption and dispersion effect are negligible compared with the L band result.

Table 1. Quantitative summary of the ionospheric effects in various frequency bands.

Effect	Frequency dependence	0.1 GHz	0.25 GHz	0.5 GHz	1 GHz	3 GHz	10 GHz
Faraday rotation	$1/f^2$	30 rotations	4.8 rotations	1.2 rotations	108°	12°	1.1°
Propagation delay	$1/f^2$	25 μs	4 μs	1 μs	0.25 μs	0.028 μs	0.0025 μs
Refraction	$1/f^2$	< 1°	< 0.16°	< 2.4′	< 0.6′	< 4.2″	< 0.36″
Variation in the direction of arrival (r.m.s.)	$1/f^2$	20′	3.2′	48″	12″	1.32″	0.12″
Absorption (auroral and/or polar cap)	$\approx 1/f^2$	5 dB	0.8 dB	0.2 dB	0.05 dB	6×10^{-3} dB	5×10^{-4} dB
Absorption (mid-latitude)	$1/f^2$	< 1 dB	< 0.16 dB	< 0.04 dB	< 0.01 dB	< 0.001 dB	$< 1 \times 10^{-4}$ dB
Dispersion	$1/f^3$	0.4 ps/Hz	0.026 ps/Hz	0.0032 ps/Hz	0.0004 ps/Hz	1.5×10^{-6} ps/Hz	4×10^{-7} ps/Hz
Scintillation(1)	See Rec. ITU-R P.531	See Rec. ITU-R P.531	See Rec. ITU-R P.531	See Rec. ITU-R P.531	> 20 dB peak-to-peak	≈ 10 dB peak-to-peak	≈ 4 dB peak-to-peak

* This estimate is based on a TEC of 10^{18} electrons/m^2, which is a high value of TEC encountered at low latitudes in daytime with high solar activity.

** Ionospheric effects above 10 GHz are negligible.

(1) Values observed near the geomagnetic equator during the early night-time hours (local time) at equinox under conditions of high sunspot number.

4. Link analysis for KNS

In this section, the detailed attenuation model is implemented and applied to the space to earth linkage considering a virtual orbit for a next generation GNSS satellite. For the virtual orbit generation and attenuation calculation, MATLAB codes were developed and simulation was performed for a one day period. Using these attenuation results, link analysis is carried out by considering candidate frequencies in the Ku and V band.

4.1 Orbit generation

For analysis of the satellite signal attenuation, we assumed two types of satellite orbits as candidates for the KNS application. Fig. 3 shows the ground trajectories of the candidate satellite orbits.

From Fig. 3 it can be observed that there are two orbit groups of satellite. The first one is a geostationary orbit (GEO) with an orbit altitude of about 35,786 km, which is accommodated in a conventional space-based augmentation system (SBAS) satellite orbit. The other is an elliptically inclined geosynchronous orbit (EIGSO) with a semi-major axis of about 42,164 km. The inclination angle and eccentricity of the EIGSO are 41 degree and 0.075, respectively. It is important to note that in the EIGSO orbit determination, satellite visibility around the Korean peninsula region is specifically taken into account. Thus, the center longitude of the EIGSO orbit is allocated at 127° E. Assuming the ground station to be in Seoul, the minimum

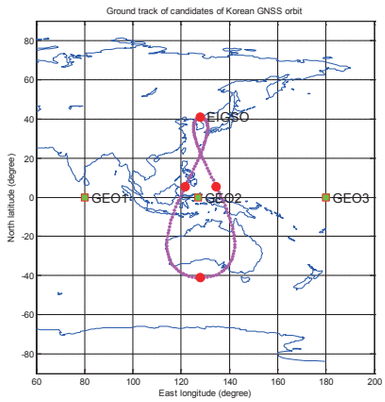

Fig. 3. KNS orbit trajectory candidates under consideration.

DOI: http://dx.doi.org/10.5139/IJASS.2016.17.1.80

and maximum distances from the chosen EIGSO are 37,034 km and 38,973 km, respectively. In the case of GEO, the range and elevation can vary according to the ground station position. Table 2 shows the intervals of each GEO satellite around the Korean peninsula area, and Fig. 4 shows the elevation and range profile of the EIGSO satellite for a one day period.

4.2 Link analysis via signal attenuation

First, the free space loss of an EIGSO for a one day period is shown in Fig. 5(a). It has a curve similar to the range profile of the EIGSO because the free space loss is logarithmically proportional to the line-of-sight distance between the EIGSO and the ground station antenna. During the visible time period, the free space loss for the signal frequency of 14.35 GHz varies with a small fluctuation between 206.91 dB and 207.35 dB. It is comparable to the free space loss of GEO that is between 206.92 dB and 207.48 dB. For the signal frequency of 44 GHz, it is approximately 10 dB higher with the range being between 216.64 dB and 217.08 dB.

The gaseous absorption is not dependent on the range but on the elevation angle of the EIGSO because its orbit is much higher than the troposphere and the elevation angle primarily determines the slant path length. Fig. 5(b) and 5(c) show the gaseous absorption in the EIGSO for the signal frequencies of 14.35 GHz and 44 GHz, respectively. In the interval between 5.25 hr and 18.67 hr when the elevation angle is higher than 45 degree, the gaseous attenuation is less than 0.2 dB for the signal frequency of 14.35 GHz, but it increases rapidly in the lower elevation interval. In the summer atmosphere, the gaseous absorption is less than 0.2 dB for 65% of the orbit period and 0.4 dB for 79% of the orbit period. Similar curves can be observed for the signal frequency of 44 GHz, but the attenuation is much higher with a minimum and maximum attenuation of 0.74 dB and 11.79 dB, respectively in the summer atmosphere.

Figure 6(a) shows the attenuation by water droplets. It is also primarily dependent on the elevation angle of the EIGSO and results in curves similar to the gaseous absorption. A statistical model is used as the water droplet density can change frequently. For example, the attenuation curve for 1% exceedance probability means that the attenuation will be less than the curve for 99% of the time in a year. For the signal

Table 2. Range and elevation window of the GEO orbits.

	GEO1	GEO2	GEO3
Range (km)	38,883~39,511	37,075~37,710	39,439~39,568
Elevation (degree)	20.4~26.9	40.8~49.9	19.8~21.1

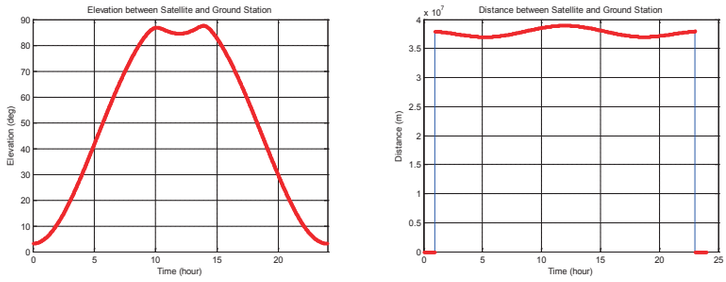

Fig. 4. Elevation and range profiles of the KNS EIGSO satellite for a one day period.

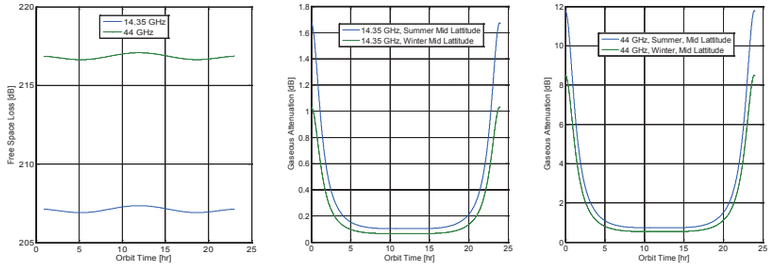

(a) (b) (c)

Fig. 5. (a) Free space loss and (b)(c) gaseous absorption for Ku and V band signals in the KNS EIGSO.

frequency of 14.35 GHz, the attenuation during the interval when the elevation angle is higher than 45 degree is less than 0.60 dB and 0.22 dB for the exceedance probabilities of 1% and 5%, respectively. However, for the signal frequency of 44 GHz, the attenuation is approximately 8 times higher.

Next, the rain attenuation is presented in Fig. 6(b). Similar statistical analysis considering rainfall probability is used. The attenuation at the signal frequency of 14.35 GHz when the elevation angle is higher than 45 degree is less than 0.65 dB and 0.09 dB for the exceedence probabilities of 1% and 5%, respectively. For the signal frequency of 44 GHz, attenuation is less than 9.5 dB and 1.8 dB for the exceedance probabilities of 1% and 5%, respectively. Thus, it can be concluded that the attenuation due to rainfall is dominant for near millimeter wave signal transmission.

Lastly, other attenuation effects including scintillation, ionospheric fading, and background noise contribute in the range of about 10^{-1}~10^{-2} dB to the total attenuation for a satellite elevation angle larger than 5 degree. Therefore, their aggregate effect is relatively negligible as compared with the dominant factors such as gas absorption and the water-associated fading effects.

4.3 System level analysis

In Fig. 7, signal attenuation is summarized for Ku and V bands through a tropospheric propagation path when the KNS EIGSO is employed. In the case of the Ku band, 14.35 GHz is taken as the carrier frequency. Mid-to-high elevation angles are essential for better link performance since an abrupt increase of tropospheric attenuation factors is observed during the low elevation angle intervals. In the analysis, a mask angle larger than 30 degree is used. Also, 1% exceedance probability, which is a moderate assumption of an unfavorable weather condition, is chosen for the analysis. It corresponds to a water droplet density of 2.344 kg/m^2 and a rainfall rate of 2.75 mm/hr. Therefore, the computed values provide the upper bound for the attenuation with 99% availability period.

In the case of Ku band, the total attenuation is about 216.7 dB and 221.2 dB for high and mid elevation angles, respectively. It is noted that gas absorption has a slight effect in the mid-to-high elevation angle condition, while the water-associated factors dominantly attenuate the signal strength. If no rain is assumed, the total attenuation decreases by 8.5 dB.

On the other hand, in the case of V band, the total attenuation is about 238.7 dB and 250.5 dB for high and mid elevation angles, respectively. Compared with the Ku band, frequency sensitive factors such as path loss and water-associated attenuations are increased significantly. However, the increase in gas absorption and scintillation is relatively negligible. In system level link analysis, the required transmitter effective isotropic radiated power (EIRP) from the satellite is about 42 dBW and 46.4 dBW in the Ku band for high and mid elevation angles, respectively. Comparatively, transmitter EIRPs of 64 dBW and 75.7 dBW are required in the V band for high and mid elevation angles, respectively. In these computations, the effective carrier to noise density ratio required from the receiver is assumed to be 45 dBHz considering conventional GPS signal tracking performance. The computed transmitter EIRP amounts to several hundred watts to several thousand watts in satellite TX power with conventional transceiver antenna gains.

Thus, it is observed that the total attenuation greatly varies according to the weather condition through the tropospheric path. The rainfall rate primarily dominates the total attenuation. Fig. 8 summarizes the predicted total attenuation and the corresponding satellite transmitter EIRP for a proper satellite navigation link performance under two rainfall conditions. The 1% and 5% exceedance probabilities amount to 2.75 mm/hr and 0.29 mm/hr rainfall rates, which

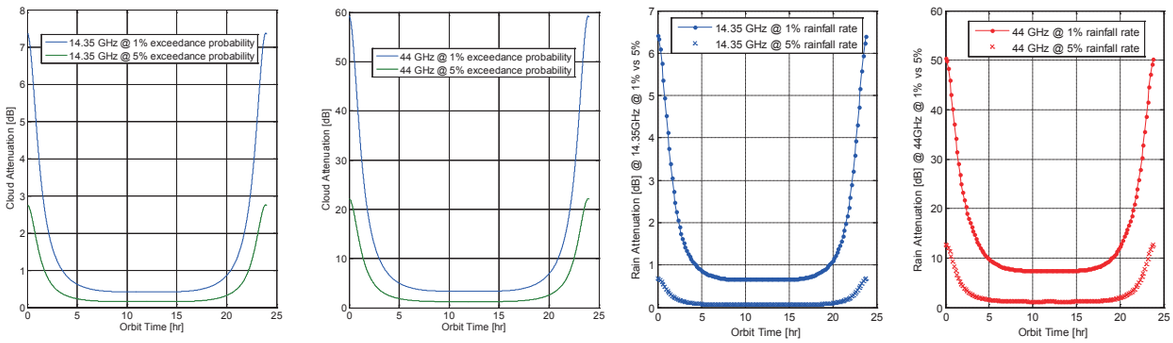

(a) (b)

Fig. 6. Attenuation by (a) cloud and (b) rainfall for Ku and V band signals in the KNS EIGSO.

DOI: http://dx.doi.org/10.5139/IJASS.2016.17.1.80

correspond to moderate and very light rainfall, respectively. Under moderate and light rainfall conditions, the Ku band carrier signal requires a proper transmitter power of several hundred watts, while the V band requires ten times higher power consumption.

Furthermore, heavy rain condition with rainfall rate higher than 30 mm/hr imposes an excessive implementation burden on the transceiver system. Using the statistical model in [18], signal attenuation at a rainfall of 30 mm/hr is computed to be 7~8 dB and 45~50 dB in the Ku and V band, respectively. This amounts to an increase in the power between space and ground transceiver system by 2 and 63 times in the Ku and V bands, respectively as compared to the results of a rainfall of 2.75 mm/hr. Consequently, the Ku band carrier is expected to provide a promising implementation candidate for the satellite navigation purpose, even considering the present power budget status of the satellite. In contrast, the V band carrier, as a millimeter wave candidate, still requires significant technical advances in satellite transceiver system design for achieving enhanced processing gains even when a light rainfall is assumed.

5. Conclusions

In this paper, the tropospheric attenuation effect on new carrier bands for a next generation satellite navigation system is investigated. Essential attenuation factors including free space loss, gas absorption, and rainfall propagation are investigated to provide an attenuation quantity for each, and as a result, a system level link analysis is performed. In the simulation study, a candidate orbit of Korean regional satellite navigation system is assumed for computing the range and elevation angle between the satellite and receiver.

System Engineering of Navigation Satellite					
Tx Frequency	**GHz**	**Ku - high**	**Ku - mid**	**V - high**	**V - mid**
Total attenuation *	**dB**	208.9	210.1	229.7	235.0
Transmitter EIRP	**dBW**	34.1	35.3	55.0	60.2
Total attenuation **	**dB**	208.3	209.2	223.4	226.3
Transmitter EIRP	**dBW**	33.5	34.5	48.7	51.5
Total attenuation ***	**dB**	208.2	209.2	222.2	224.5
Transmitter EIRP	**dBW**	33.5	34.4	47.5	49.7
* 2.75 mm/hr, 1% probability					
** 0.29 mm/hr, 5% probability					
*** No rain					

Fig. 8. Navigation satellite's power budget comparison under different rainfall conditions (KNS EIGSO case).

Through a link budget analysis for the new band carriers, power requirement of the satellite transmitter is presented and system feasibility is analyzed considering the critical weather conditions such as gas absorption, water droplets, and rainfall effects.

Acknowledgments

This paper was written as part of Konkuk University's research support program for its faculty on sabbatical leave in 2013 and the National GNSS Research Center program of Defense Acquisition Program Administration and Agency for Defense Development.

References

[1] Thevenon, P., Bousquet, M., Macabiau, C., Grelier, T., Ries, L. and Roviras, D., "Regulatory Analysis of Potential Candidate Bands for the Modernization of GNSS Systems in 2015-2020", *Proceedings of IEEE IWSSC*, 2008, pp. 172-175.

[2] Hein G. W., Avila-Rodriguez, J. A., Wallner S., Eissfeller B., Isigler M. and Issler, J. L., "A vision on new frequencies,

Tx Frequency	**GHz**	**14**		**44**		Note
Max. EIRP	**dBW**	**42.0**	**46.4**	**64.0**	**75.7**	
Diameter of footprint(nadir)	km					
Pointing loss	dB	0.8	0.8	0.8	0.8	thetaTX=theta_3dB/4
coupling/insertion loss	dB	1.5	1.5	1.5	1.5	
Effective EIRP	**dBW**	**39.8**	**44.2**	**61.8**	**73.5**	
Elevation angle	deg	> 60	> 40	> 60	> 40	mask angle > 30 deg
Slant range	km	37034.0	38973.0	37034.0	38973.0	min - max range
Path loss	dB	206.9	207.4	216.6	217.1	
Gas	dB	0.1	0.2	0.8	1.2	H2O and O2 gas
Rainfall*	dB	8.5	12.0	16.5	26.0	1% exceedence probability
Cloud/fog **	dB	0.4	0.6	3.8	5.0	1% exceeding probability
Scintillation/etc... ***	dB	0.8	1.0	1.0	1.2	worst case scintillation, 0.3m foliage
ionospheric fading	dB	0.0	0.0	0.0	0.0	
Total Attenuation	**dB**	**216.7**	**221.2**	**238.7**	**250.5**	
Rx Antenna Gain	dB	24.0	24.0	24.0	24.0	
Implementation loss	dB	6.0	6.0	6.0	6.0	
Thermal noise floor @ Temp_R	dB	-204	-204	-204	-204	
Effective C/N0 (tracking loop) ****	**dBHz**	**45.0**	**45.0**	**45.0**	**45.0**	
* rainfall rate = 2.75 mm/hr						
** water cumulant =2.344 kg/m^2						
*** worst case scintillation, 0.3m foliage						
**** GPS L1 Receiver tracking requirement : ~45 dBHz						

Fig. 7. Attenuation by cloud and rainfall for Ku and V band signals in the EIGSO.

signals and concepts for future GNSS systems", *Proceedings of ION GNSS 2007*.

[3] Mateu, I., Boulanger, C., Issler, J. L., Ries, L., Avila-Rodriguez, J. A., Wallner, S., Kraus, T., Eissfeller, B., Mulassano, P., Caporate, M., Germaine, S., Guyomand, J. Y., Bastide, F., Godet, J., Hayes, D., Serant, D., Thevenon, P., Julien, O. and Hein, G., "Exploration of Possible GNSS Signals in S-band", *Proceedings of 22nd International Meeting of the Satellite Division of The Institute of Navigation*, Savannah, GA, September 22-25, 2009, pp. 1573-1587.

[4] Irsigler, M., Hein, G. W. and Schmitz-Peiffer, A., "Use of C-Band frequencies for satellite navigation: benefits and drawbacks", *GPS Solutions*, Vol. 8, No. 3, 2004, pp.119-139.

[5] FCC ONLINE TABLE OF FREQUENCY ALLOCATIONS, FEDERAL COMMUNICATIONS COMMISSION OFFICE OF ENGINEERING AND TECHNOLOGY, POLICY AND RULES DIVISION 47 C.F.R. § 2.106, Revised on April 16, 2013

[6] Liebe, H. J., "MPM - An atmospheric mm-wave propagation model", *International Journal of Infrared and Millimeter Waves*, Vol. 10, No. 6, 1989, pp. 631-650.

[7] Schneider, T., "Link Budget Analysis for Terahertz Fixed Wireless Links", *IEEE Tr. On Terahertz Science and Technology*, Vol. 2, No. 2, 2012, pp. 250 – 256.

[8] Espeland, R. H., Violette, E. J. and Allen, K. C., "Atmospheric Channel Performance Measurements at 10 to 100 GHz", NTIA Technical Report TR-84-149, April 1984

[9] Dees, J. W., King, J. L. and Wiltse, J. C., "A millimeter wave propagation experiment from the ATS-E spacecraft", NASA Technical Report NASA-TM-X-60763, 1967 and presented at IEEE, Group On MICROWAVE THEORY AND TECH.; 18-21 MAR. 1968; NEW YORK

[10] Fugono, N., Yoshimura, K., & Hayashi, R., "Japan's Millimeter Wave Satellite Communication Program", IEEE Tr. *On Communications*, Vol. 27, No. 10, 1979, pp. 1381-1391.

[11] Antes, J., Reichart, J., Lopez-Diaz, D., Tessmann, A., Poprawa, F., Kurz, F. and Kallfass, I., "System concept and implementation of a mmW wireless link providing data rates up to 25 Gbit/s", *Proceedings of the IEEE COMCAS*, Tel Aviv, Israel, 2011.

[12] Castanet, L., Lemorton, J., Konefal, T., Shukla, A. K., Watson, P. A. and Wrench, C. L., "Comparison of Various Methods for Combining Propagation Effects and Predicting Loss in Low-Availability Systems in the 20-50 GHz Frequency Range", *Int'l. J. Satell. Commun.*, Vol. 19, Vol. 3, 2001, pp. 317–334.

[13] Propagation data and prediction methods required for the design of Earth-space telecommunication systems, Recommendation ITU-R P.618-11 (09/2013)

[14] Specific attenuation model for rain for use in prediction methods, Recommendation ITU-R P.838-3

[15] Attenuation by atmospheric gases, Recommendation ITU-R P.676-10 (09/2013)

[16] Attenuation due to clouds and fog, Recommendation ITU-R P.840-6 (09/2013)

[17] Ionospheric propagation data and prediction methods required for the design of satellite services and systems, Recommendation ITU-R P.531-12 (09/2013)

[18] Characteristics of precipitation for propagation modeling, Recommendation ITU-R P.837-6 (02/2012)

[19] Rain height model for prediction methods, ITU-R P.839-4 (09/2013)

[20] The radio refractive index: its formula and refractivity data, Recommendation ITU-R P.453-10 (02/2012)

[21] A general purpose wide-range terrestrial propagation model in the frequency range 30 MHz to 50 GHz, Recommendation ITU-R P.2001 (02/2012)

[22] Guide to the application of the propagation methods of Radiocommunication Study Group 3, Recommendation ITU-R P.1144-6 (02/2012)

DOI: http://dx.doi.org/10.5139/IJASS.2016.17.1.80